Q. J. R. Meteorol. Soc. (1993), **119**, pp. 733–754 551.553.21:551.515.1:551.515.4(94)

An integrated view of the 1987 Australian monsoon and its mesoscale convective systems. II: Vertical structure

By BRIAN MAPES* and ROBERT A. HOUZE, JR.
University of Washington, USA

(Received 14 April 1992; revised 17 November 1992)

SUMMARY

The vertical structure of monsoon thermal forcing by precipitating convection is diagnosed in terms of horizontal divergence. Airborne Doppler-radar divergence profiles from nine diverse mesoscale convective systems (MCSs) are presented. The MCSs consisted of multicellular convective elements which in time gave rise to areas of stratiform precipitation. Each of the three basic building blocks of the MCSs—convective, intermediary, and stratiform precipitation areas—has a consistent, characteristic divergence profile. Convective areas have low-level convergence, with its peak at 2–4 km altitude, and divergence above 6 km. Intermediary areas have convergence aloft, peaked near 10 km, feeding into mean ascent high in the upper troposphere. Stratiform areas have mid-level convergence, indicating a mesoscale downdraught below the melting level, and a mesoscale updraught aloft.

Rawinsonde composite divergence profiles agree with the Doppler data in at least one important respect: the lower-tropospheric convergence into the MCSs peaks 2–4 km above the surface. Rawinsonde vorticity profiles show that monsoonal tropical cyclones spin-up at these elevated levels first, then later descend to the surface. Rawinsonde observations on a larger, continental scale demonstrate that at large horizontal scales only the 'gravest vertical mode' of MCS heating is felt, while the effects of shallower components of the heating (or divergence) profiles are trapped near the heating, as predicted by geostrophic adjustment theory.

1. INTRODUCTION

Tropical deep convection constitutes the diabatic ascending branch of planetary-scale mean tropical circulations, such as the Hadley and Walker circulations. As a result its mean properties have great importance to weather and climate on even the largest space- and time-scales. In addition a variety of more transient disturbances, such as easterly waves, depressions and cyclones, the monsoons and the intraseasonal oscillation modulate, and are modified by, their embedded deep convection. Of particular importance is the vertical structure of the heating in mesoscale convective systems (MCSs). This paper utilizes both Doppler-radar measurements within tropical MCSs, and rawinsonde measurements on larger scales, in considering the vertical structure of convective heating and the resulting monsoon wind systems.

The Australian monsoon of 1987, as observed by the Australian Monsoon Experiment (AMEX) (Gunn *et al.* 1989) and the Equatorial Mesoscale Experiment (EMEX) (Webster and Houze 1991; Mapes and Houze 1992, hereafter Part I), provided an excellent natural laboratory for investigating at various spatial scales the processes at work in a highly convective area of the tropical troposphere. AMEX and EMEX were conducted concurrently during January and February of 1987 (Part I; Webster and Houze 1991). In contrast to the easterly wave regimes of many previous tropical field programs, there was essentially no background mean flow through the Australian monsoon area. Rather, the mean flow was the monsoon's own circulation: a cyclonic gyre in the lower troposphere and an anticyclonic gyre in the upper troposphere (Figs. 3 and 4 in Part I). The evolution of the monsoon flow consisted of multi-day periods of convective activity, acting to spin-up low-level cyclones, which in turn organized the convection (Figs. 8 and 9 of Part I). Ultimately these monsoon cyclones achieved hurricane strength before dissipating at landfall. Ten MCSs, in various temporal and spatial parts of this cycle of activity, were extensively studied with multiple aircraft and airborne Doppler radar.

* Corresponding author: Department of Atmospheric Sciences, AK-40, University of Washington, Seattle, Washington 98195, USA.

In Part I we presented observations of the horizontal structure of the 1987 Australian monsoon and its associated MCSs. Upscale forcing of the monsoon circulation by embedded MCSs was examined from the point of view of vorticity, which is affected by MCSs in two ways. Most prominently the divergence* associated with net MCS heating 'stretches' vorticity at many scales, acting to spin-up the regional and planetary monsoon circulations, as well as the embedded mesoscale vortices, depressions and tropical cyclones. This divergent flow is the subject of the present paper. The other effect of MCSs on vorticity is that their upward momentum transport creates vortex couplets in the upper troposphere (Fig. 6(c) of Part I).

Houze (1982, 1989) examined the heating processes active in MCSs and reviewed a large body of relevant observations. Condensation in updraughts and evaporation in downdraughts are the major contributors, so that the fluid dynamics (e.g. entrainment) governing profiles of vertical mass flux are inseparable from the thermodynamic processes (water phase change) which constitute the heating. In a diagnostic framework, then, 'measurements' of tropical MCS heating essentially consist of estimates of vertical mass fluxes, derived in turn from estimates of the divergence of measured winds. Divergence profiles are integrated vertically to yield vertical velocity or heating profiles. This process de-emphasizes high vertical wave-number features of the divergence profile, and vertically smears errors in the divergence measurement at one level to all levels in the resulting heating profile. Hence, heating profiles tend to look similar, and differences among them are difficult to interpret.

In this paper we focus directly on divergence. A large set of airborne Doppler-radar data, within nine different MCSs in various synoptic settings within the monsoon, shows that divergence profiles within convective, intermediary, and stratiform precipitation areas are remarkably consistent from case to case. The rawinsonde composite data used by Frank and McBride (1989) are reanalysed in terms of divergence, and an important feature, also present in the Doppler divergence profiles, emerges: *the net low-level convergence into monsoon MCSs has its maximum elevated off the surface*. A similar elevated convergence appears in composite divergence profiles for mid-latitude mesoscale convective complexes (Fig. 7 of Maddox 1983). This fact has at least two important consequences: it indicates that these MCSs should cause boundary-layer area contraction in their environment (Mapes 1993), and that monsoonal tropical cyclones initially spin-up aloft, and then later descend to the surface (see Fig. 10; Davidson *et al.* 1990).

Section 2 details the data and methods used in this study, including a new Doppler-radar processing methodology. In section 3 the relationship between horizontal divergence, which can be measured, and heating, which cannot, is reviewed. Results are presented from the large and unique EMEX airborne Doppler-radar data set in section 4. Section 5 presents larger-scale rawinsonde-based divergence and vorticity measurements.

2. Data and methods

The data for this study are essentially of two types: airborne Doppler-radar data, which we have used to measure the divergence within MCSs, and soundings around the north Australian region (Fig. 1), which we have used to evaluate the vertical structure of the synoptic flow. The soundings were obtained in AMEX.

The Doppler-radar data were collected in EMEX, aboard the US National Oceanic and Atmospheric Administration (NOAA) WP-3D research aircraft number N43RF (hereafter 'the P3'), held in the vicinity of Darwin, Australia in Jan.–Feb. 1987 (Webster

* The term 'divergence' in this paper refers to horizontal divergence.

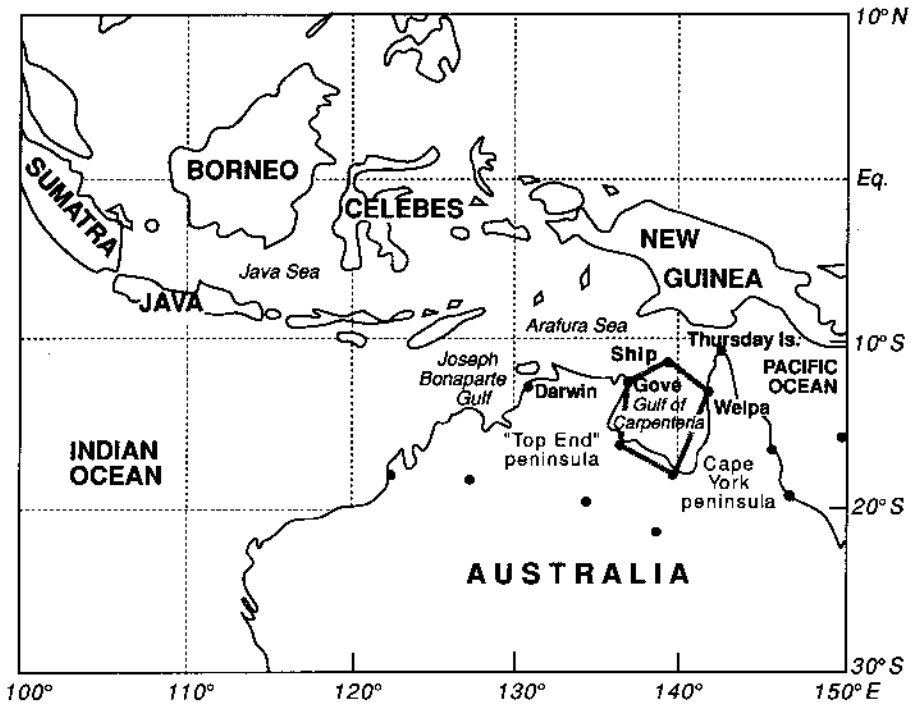

Figure 1. Base map of northern Australia and surrounding area. Heavy dots denote AMEX sounding sites. Striped line is Gulf of Carpentaria rawinsonde array.

and Houze 1991). The antenna of the tail Doppler radar of the P3 rotated at ten revolutions per minute in the vertical plane perpendicular to the aircraft track. Since the air speed of the aircraft was around 130 m s^{-1}, this means that successive sweeps of the radar were about 800 m apart. Doppler data were collected between 0.9 and 39.3 km, in 256 range bins of 150 m in length. The flight path of the P3 during Doppler sampling was a zigzagging pattern of straight legs of about 75 km (9 min) in length, typically at around 5 km altitude, oriented at approximately 60° to each other, with outside turns (Fig. 2). The sampling strategy is explained further in Webster and Houze (1991).

Area-mean horizontal divergence was calculated using Stokes's theorem:

$$\iint_A \nabla \cdot \mathbf{V}\, dA = \oint_{\mathscr{L}} \mathbf{V} \cdot \hat{\mathbf{n}}\, d\mathscr{L} \tag{1}$$

where $\mathbf{V}$ is the horizontal wind, $\hat{\mathbf{n}}$ the horizontal unit vector normal to the line integral boundary, $d\mathscr{L}$ a length element along the boundary, and A the area enclosed within the boundary $\mathscr{L}$. In this case the boundary in question is the parallelogram shown by the solid line in Fig. 2(a). The sides of this parallelogram were chosen to be perpendicular to the horizontal projections of the radar beams, and hence parallel to the flight tracks, so that the component of the wind normal to the boundary of the parallelogram is simply the horizontal component U_n of the Doppler radial velocity. Since the radar scanned in the vertical, the edges of the parallelogram are really vertical 'walls,' and the integral (1) was performed in discrete layers in the vertical, 1 km in depth, yielding profiles of divergence. The 1 km depth was chosen because the radar beam width (1.9°) is about 1 km at 30 km range.

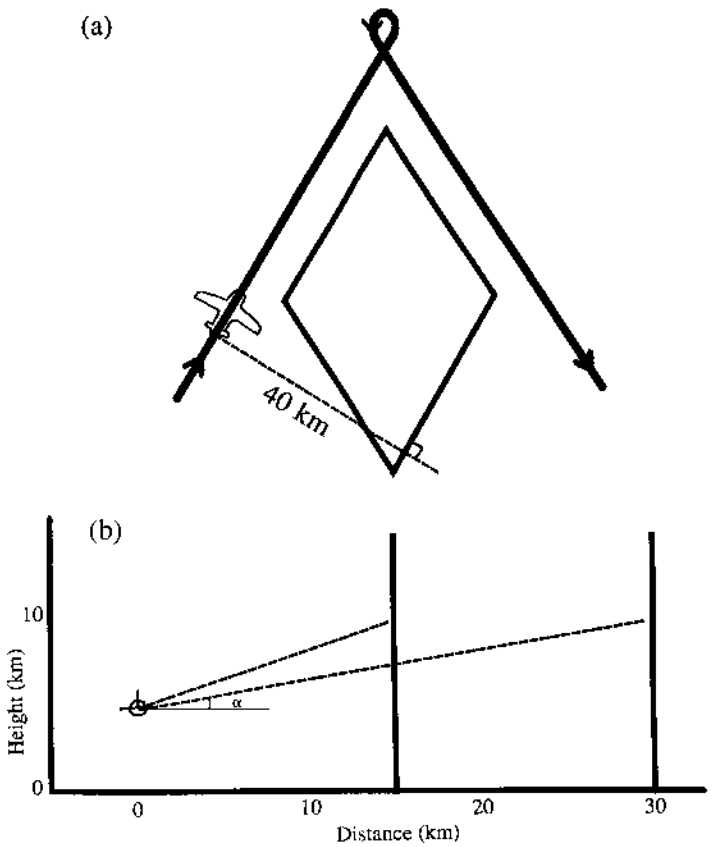

Figure 2. Geometry of the airborne Doppler divergence measurement, (a) in plan view and (b) vertical cross-section. Dashed lines indicate radar beams, with α the elevation angle of Eq. (2).

The horizontal component of the Doppler radial velocity was estimated from the actual radial velocity, as illustrated in Fig. 2(b). For radar beams at elevation angle α, the horizontal component U_n is given by:

$$U_n = \{V_r - (w - V_t)\sin(\alpha)\}/\cos(\alpha) \tag{2}$$

where V_r is Doppler radial velocity, w is the vertical air velocity, and V_t is the reflectivity weighted terminal fall speed of radar scatterers. In our calculations we have neglected the term $w\tan(\alpha)$, and estimated V_t from radar reflectivity according to the formulae used by Marks and Houze (1987). An upper limit on the divergence error implied by a constant $1\,\mathrm{m\,s^{-1}}$ error in the assumed $(w - V_t)$ can be estimated from one-dimensional considerations in this same geometry:

$$\delta\mathrm{div} \sim \delta U_n/\delta x \sim 1\,\mathrm{m\,s^{-1}}\,[\delta z/r_1 - \delta z/r_2]/(r_2 - r_1) = 1.8 \times 10^{-5}\,\mathrm{s^{-1}} \tag{3}$$

where δz (taken as 7 km) is the maximum height of the divergence calculation above or below flight level, and r_1 and r_2 (taken as 10 and 40 km) are the horizontal distances from the aircraft to the near and far walls respectively (Fig. 2(b)). In calculating each divergence profile the expected apparent divergence (EAD) due to the V_t—convergence below the flight level, divergence above—was used to adjust the calculated values. In general the EAD was much smaller than the measured divergences (see Fig. 6), unless

the closer wall was put too close to the flight track. Data with elevation angles exceeding ±45° were, therefore, never used.

The edges ('walls') of the parallelograms were chosen subjectively, within the constraints of the 45° elevation cut-off, the Doppler range limit, and the area of available Doppler data (precipitation area). Generally these areas were about 500 km^2, so the profiles should be interpreted as representing areas of linear dimension ~22 km. Experience shows that the results are not overly sensitive to the exact location of the parallelogram. For each parallelogram the divergence calculation was done with threefold redundancy: the locations of the parallelogram walls were shifted by one Doppler-radar range interval (150 m) each way to obtain three profiles, from completely independent data but with negligibly different geometry. This redundancy has been carried through all calculations and can be seen in the profiles below (Figs. 6–8); the spread of the three estimates reflects the small fraction of the variability which is due to sampling error.

The time necessary to fly the zigzag pattern shown in Fig. 2(a) was about 15–20 minutes. A correction for spatial translation during the data collection period was made, based on subjective evaluation of the motion of features in the reflectivity field. The effect of this correction on the results was small. It is impossible to evaluate the effect on our results of other forms of evolution more complicated than linear spatial translation during the data collection period. However, the consistency of the results from case to case leads us to believe that for the 500 km^2 (approx.) horizontal scale inherent in the method, the mean structure lasts long enough to be well sampled.

The integral (1) was evaluated at each level by using all available data on each of the four 'walls' to evaluate the mean cross-wall velocity, and then summing these four mean velocities, weighted by the lengths of the walls. In this process it was not necessary to synthesize multiple-Doppler radial velocity estimates, collected at different times and from different vantage points, to obtain vector-wind estimates. As a result, interpolation error was eliminated, and much computer time was saved. The rapidity of the calculation permitted interactive graphical processing. Because a relatively small amount of data was used, and used in its raw form, it was easy to visually inspect and edit all data which entered the calculation. In addition the process employed none of the 'black box' filtering and iterative calculations traditionally used in Doppler-radar processing, so that surprising and interesting results could be quickly and unambiguously traced back to the raw observations.

Sampling was poor in the upper troposphere because the 3 cm wavelength radar suffered attenuation on long slant paths through precipitation. This effect accounts for increasing differences among the three estimates above 10 km altitude in Figs. 6–8. The tops of the observed MCSs were considerably higher than 10 km, typically 14–16 km or more, according to vertical-incidence radar data and cloud-top temperatures inferred from infrared satellite data.

In the lowest layer, 0–1 km, special problems arose. Since the radar beam width (full width at half power) was 1.9°, some power was returned by the sea surface, especially at far ranges. The effect of sea-surface echo on radial velocity depends on the relative contributions to the radar reflectivity of the precipitation particles and the sea surface. Sea-surface reflectivity is a function of sea state, and is higher for upwind-looking beams than downwind-looking beams. In general the presence of sea clutter tends to bring radial velocities of either sign closer to zero. The effect of sea clutter on the divergence profiles, therefore, depends on wind speed, and on the orientation of the parallelogram with respect to wind direction. In short we could find no simple objective way to remove or correct for sea clutter, so divergence in the lowest layer must simply be viewed as subject to special uncertainty.

3. Heating, vertical velocity, and divergence

While it may be convenient in theoretical and modelling work to formulate the equations governing atmospheric flow in terms of heating, this convention is not ideal for the interpretation of observations. Heating is an impossible quantity to measure directly, and is instead typically diagnosed using the thermodynamic equation, here in isobaric coordinates:

$$\frac{\partial T}{\partial t} + \mathbf{U}\cdot\nabla\mathbf{T} = \omega\sigma + Q_1 \tag{4}$$

where $\mathbf{U}$ is the horizontal wind, ω is the rate of change of pressure, p, following fluid motion, σ is the static-stability parameter $(T/\theta)\,(\partial\theta/\partial p)$ where T is temperature and θ is potential temperature, and Q_1 is the heating rate in degrees per unit time, t.

If temperature varies little from time to time and place to place, as is observed in the tropics on scales larger than convective, then the left-hand side is small and the static stability σ is a nearly constant proportionality factor between ω and Q_1. Q_1 is called the 'apparent heat source,' defined by (4) when ω is taken to be the mean vertical velocity *as resolved by the measurements in question*. In the case where ω represents mesoscale or synoptic-scale mean vertical motion, Q_1 includes eddy heat transports by unresolved convective transports (cancelling up and down motions with unequal temperatures), as well as actual heating by water phase changes and radiative energy flux divergence. The close correspondence of Q_1 and ω can be seen in Fig. 3, adapted from Frank and McBride's (1989) composite rawinsonde heat budget of mature Gulf of Carpentaria MCSs during AMEX/EMEX. Of course the apparent heating and vertical velocity shown in the figure are not independent. What Fig. 3 really shows is that large-scale temperature advection is small (Frank and McBride did not even attempt to estimate the small storage term $\delta T/\delta t$) and that σ does not vary much with height through most of the troposphere (though it decreases rapidly above about 350 mb).

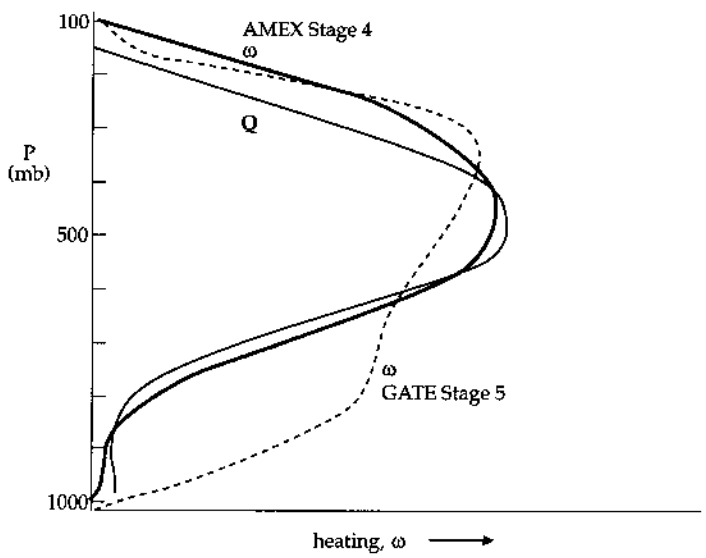

Figure 3. Comparison of heating (Q, in temperature/time units) and vertical-velocity (ω, in pressure/time units) profiles for composite mature MCSs in the Gulf of Carpentaria. GATE mature MCS ω profile shown for comparison. Adapted from Frank and McBride (1989).

Vertical velocity is notoriously difficult to measure. MCSs contain a broad spectrum of individual vertical velocities, both upward and downward, especially but not solely in the very active convective portions of the system. To illustrate this, Fig. 4 shows histograms of hydrometeor vertical velocity* at various altitudes from the P3 Doppler-radar data at vertical incidence. Each flight leg (9 min or so) in the sample has been subjectively classified as convective, intermediary, or stratiform as discussed in section 4 later, to illustrate the narrowing of the vertical-velocity spectrum with time as precipitation areas age. The means of the convective, intermediary, and stratiform histograms are not significantly different, and reflectivity based particle fall-speed corrections do not

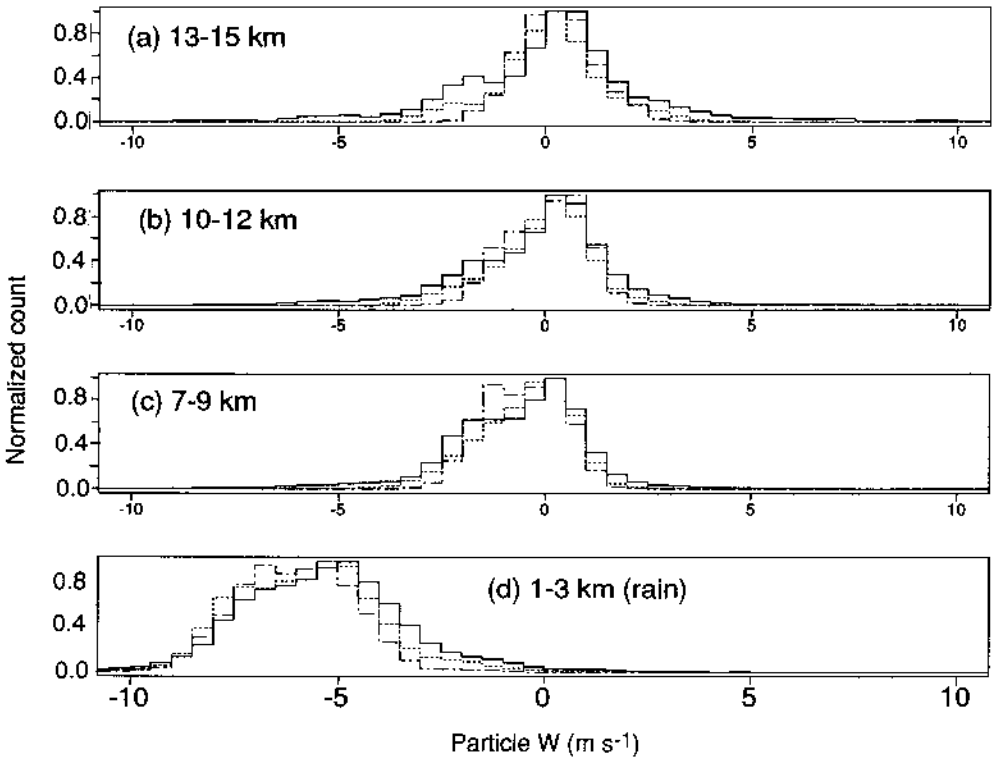

Figure 4. Normalized number histograms of W, the vertical velocity of hydrometeors (radar scatterers), in the four indicated altitude ranges, from vertical incidence airborne Doppler-radar data in four vigorous MCSs (EMEX flights 3, 6, 7, and 10). The three superposed histograms at each altitude are subsets of the data, leg by leg, subjectively classified (see text) as convective (solid lines, 22 legs), intermediary (dashed lines, 19 legs), and stratiform (dash-dot, 21 legs). The total number of independent Doppler measurements in each category is approximately 10000 in the 1–3 km altitude interval and 20000 in each of the 2 km intervals.

help. *Average vertical air velocity apparently cannot be reliably estimated by averaging a large number of vertical incidence Doppler-radar measurements.* Even *in situ* aircraft measurements of vertical air velocity typically do not have an accurate mean value.

Yet these chaotic masses of updraughts and downdraughts do average out to repeatable, consistent mean vertical mass-flux profiles, as indicated by measurements of horizontal divergence (section 4). While the numerous small-scale strong updraughts and

* No correction for hydrometeor fall speed was applied because of the uncertainty in such estimates, especially in the tropical upper troposphere where microphysical measurements have not been made. Rough values are 1 m s^{-1} for snow and 7–8 m s^{-1} for rain.

downdraughts are important contributors to the vertical eddy fluxes of hydrometeors (the 500 km^2 mean convective-area ascent rate of about 1 m s^{-1} could not loft a raindrop), along with horizontal momentum (e.g. LeMone 1983), and to a lesser degree sensible heat (e.g. Houze 1982, 1989; Jorgensen and LeMone 1989), their mass fluxes nearly cancel. The residual sum of the updraught and downdraught mass fluxes is the much smaller in magnitude, but stable and physically determined with its important relationship (4) to total heating (which includes the convective heat fluxes).

As noted above, divergence is the primary measurement underlying nearly all diagnoses of vertical velocity and heating.* Another desirable property of divergence is its role as the thermal forcing term in the equation for the vertical component of vorticity (from Eq. 2 of Part I):

$$\frac{\partial \zeta_a}{\partial t} + \mathbf{U} \cdot \nabla_p \zeta_a = -\zeta_a (\nabla_p \cdot \mathbf{U}) - \hat{\mathbf{k}} \cdot \nabla_p \times \mathbf{M}. \tag{5}$$

Here ζ_a is absolute vorticity, $\mathbf{U}$ is horizontal wind, $\hat{\mathbf{k}}$ is the vertical unit vector, and $\mathbf{M}$ represents the apparent momentum source arising from vertical momentum transports. $\mathbf{M}$ is dominated by upward transports of low-level momentum in MCSs. These upward transports create, by the second source term in (5), vortex couplets in the upper troposphere, straddling the MCSs, in which $\mathbf{M}$ is large (see, for example, Fig. 6(c) of Part I). The first source term in (5), on the other hand, represents the divergent flow associated with the net heating in MCSs. This divergent flow spans many decades of horizontal scale, and acts to spin-up both the large-scale monsoon flow and the embedded smaller-scale depressions and cyclones. Vorticity equations like (5), with divergence as the thermal forcing term, have been elegantly and profitably utilized in the study of large-scale tropical flows by Sardeshmukh and Held (1984) and Sardeshmukh and Hoskins (1985, 1987, 1988). The large-scale flow is mostly rotational, so the first source term in (5) embodies the upscale effect of MCS heating on the large-scale flow. It is clear from this that what the large scale ultimately feels from MCS heating is the associated divergence.

4. Doppler-radar divergence profiles in tropical MCSs

As illustrated in Webster and Houze (1991) and in Part I, EMEX included airborne Doppler-radar sampling of ten MCSs within various parts of the monsoon system. Using the technique outlined in section 2, we have obtained 93 divergence profiles within nine of the ten MCSs (the weak line of convection sampled on flight 2 had so little stratiform precipitation during most of the flight that Doppler-radar sampling was inadequate). These profiles can be grouped into three categories, which describe the character of the precipitation in the portions of the MCS in which the profiles were obtained. The three categories are *convective* areas, *stratiform* areas, and areas undergoing evolution from the former to the latter, which we will denote as *intermediary* precipitation areas.

Convective areas have vertically extensive high reflectivity cores or cells, delineated by large horizontal reflectivity gradients, and an irregular echo top. Stratiform areas, by contrast, have a reflectivity field with relatively little horizontal variability, a flat or smoothly sloping top, and a radar bright band at the melting level. A convective area occurs in the early stages of development of a precipitation feature within an MCS. As a convective area ages (on a time-scale of half an hour to an hour), the crisp cellular

* An exception is the wind-profiler data of Balsley *et al.* (1988). As shown by Houze (1989) the Balsley *et al.* (1988) result is quite different from all other previously reported diagnosed vertical velocities in tropical precipitation.

high-reflectivity rainshaft structures are replaced by an increasingly smooth field with some residual granulations and irregularities. This type of area we have termed *intermediary*, not only because its instantaneous radar-echo structure is intermediate between convective and stratiform, but also because it lies between convective and stratiform precipitation in a temporal sequence. As time progresses, the irregularities decrease until, 2–3 h after the initial convection, the radar echo is characteristic of stratiform precipitation. (Not all stratiform precipitation forms in this way. In some cases, upper-level shear creates an anvil cloud which later begins to precipitate.) The three precipitation types described here generally coexist in a mature MCS, whose total life cycle is much longer than the above-described life cycle of a single precipitation feature (for further discussion, see Part I).

To illustrate better the meaning of our categories we present here some individual profiles in their mesoscale meteorological context before presenting averaged profiles.

(*a*) *An example: EMEX* 6

A good example of precipitation areas undergoing evolution from convective to stratiform structure may be found in the MCS sampled during the sixth EMEX flight on 27 January 1987. It existed in a weak depression with light winds. The same geographical area was sampled repeatedly by the radar aboard the P3 aircraft while the precipitation evolved from predominantly convective to predominantly stratiform. Radar-reflectivity evolution is shown in Fig. 5, with corresponding divergence profiles shown in Fig. 6. An initial broad east–west line of echoes along 12.5–13°S (Fig. 5(a)) evolved gradually into stratiform precipitation (Fig. 5(d)). During the same period a north–south line of convection developed along the western edge of this area, and it can be seen protruding north from the sampled precipitation area in Fig. 5(d). Note that this sampled stratiform precipitation was formed in place by the evolution of prior convection, not advected or sheared off of the convective line which happened to be adjacent to it at the time of Fig. 5(d).

In the earliest profile, at 2126 GMT (Fig. 6(a)), a strong signature of deep convection (low-level convergence, upper-level divergence) is seen. By 2148 GMT, the reflectivity field was still quite granulated but no longer exhibits strong convective cells (Fig. 5(b)). We classified this precipitation area as intermediary. Its divergence profile consists of a thin layer of strong divergence at the surface, with deep convergence, to 12 km altitude at least, above that (Fig. 6(b)). The constraint of mass balance suggests that strong divergence must have existed above 12 km, as is evident in rawinsonde divergence profiles (e.g. Fig. 11). An hour later, at 2254 GMT, the convergence remained only near 10 km (Fig. 6(c)).

By 2317 GMT the signature of a lower-tropospheric mesoscale downdraught (convergence near the melting level, divergence below) had developed, but the convergence at 10 km is still evident (Fig. 6(d)). This profile is similar to the stratiform divergence profile in Fig. 6 of Srivastava *et al.* (1985). Just to the west, at 2328 GMT, the measured profile was more typical of stratiform precipitation areas (Houze 1989), with divergence up to 3–4 km altitude, convergence to 8–9 km, and divergence above that (Fig. 6(e)).

(*b*) *Mean Doppler divergence profiles*

We have subjectively grouped the 93 measured profiles into the three categories described above: convective, intermediary, and stratiform. We can think of no simple, satisfactory objective scheme for doing so, primarily because considerations include not only the instantaneous radar reflectivity pattern but also its evolution. The convective profiles represent collections of convective cells embedded in stratiform precipitation; as

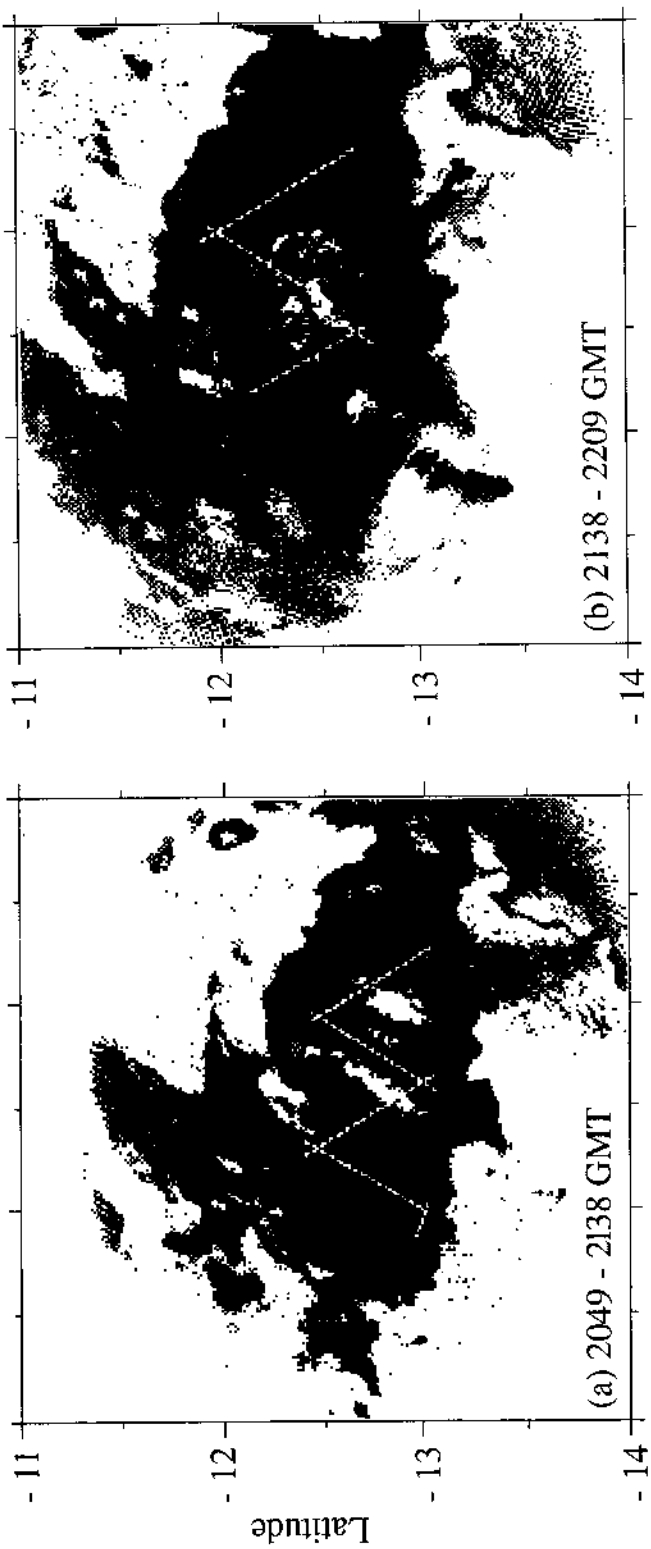

Figure 5. Radar-reflectivity time-composite images from the indicated time intervals during EMEX flight 6 on 27 January 1987. The reflectivity shown at each point is the maximum observed during the interval. Flight tracks during the intervals are shown in white, and proceed left to right in (a), right to left in (b), etc. Ground clutter at lower right.

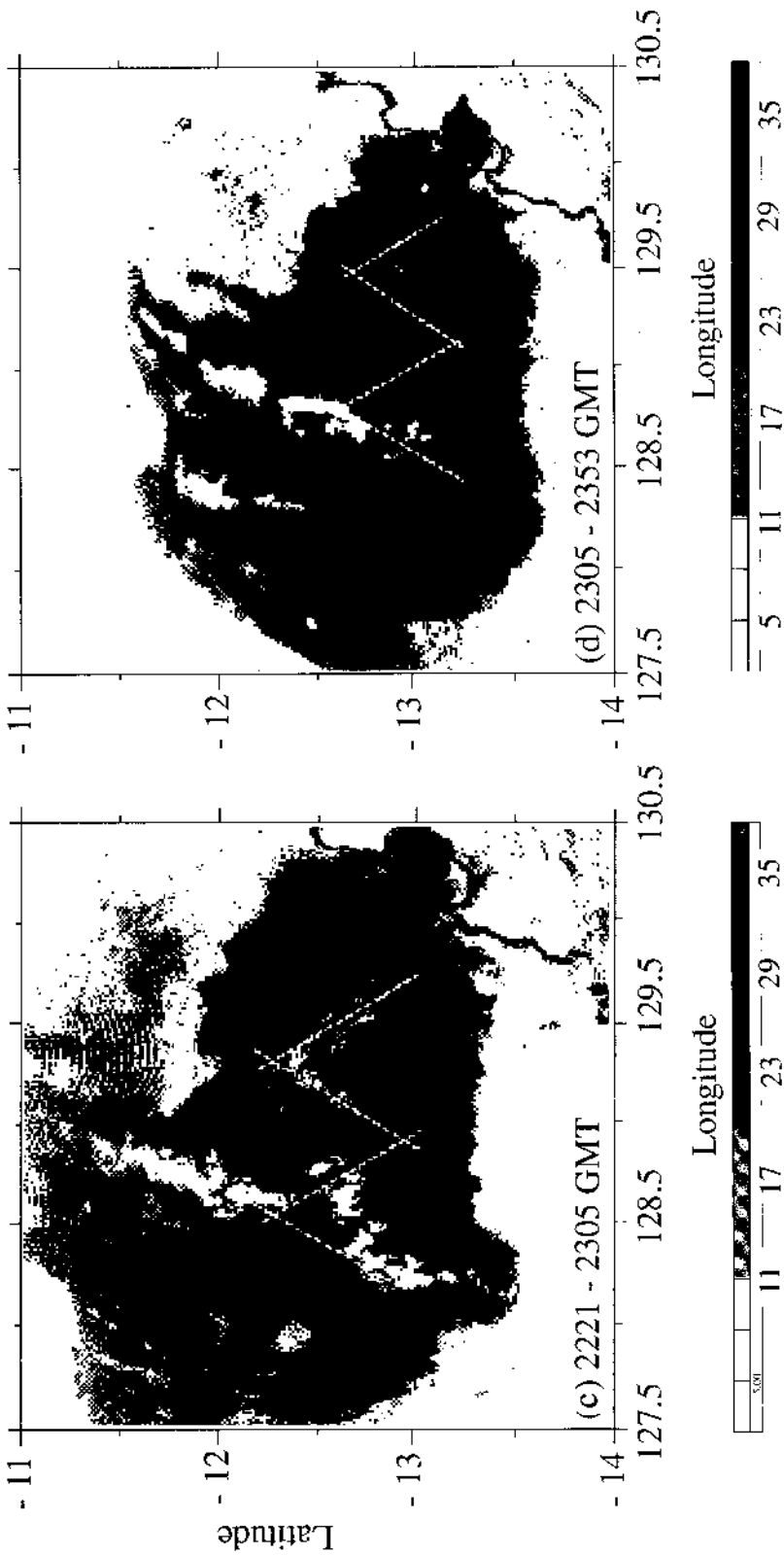

Figure 5. Continued.

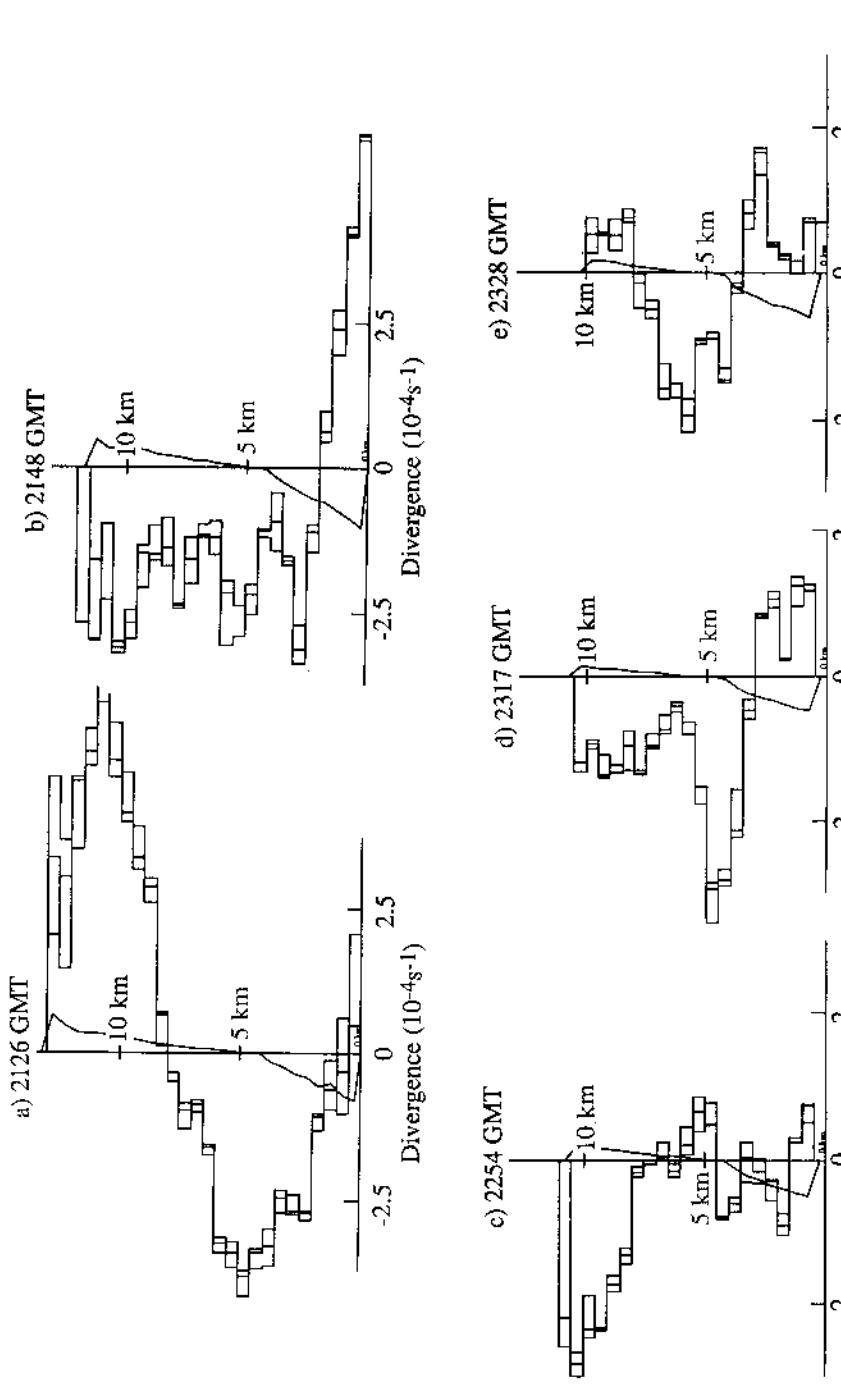

Figure 6. Profiles of horizontal divergence measured by Doppler radar during EMEX flight 6 (see Fig. 5). The three blocked lines in each plot indicate three independent Doppler estimates of mean divergence, for three areas of negligibly different geometry. The single solid line is the expected apparent divergence, calculated from reflectivity estimated particle fall speeds (see Eq. (3)), which has been subtracted from the measurements to yield actual divergence. (a–d) are for parallelograms as in Fig. 2 within the rightmost inverted-V-shaped flight tracks on (a–d) of Fig. 5, while (e) is for the parallelogram within the upright-V-shaped flight track in Fig. 5(d).

discussed above, the presence or absence of reflectivity cells is a fairly unambiguous indication of convection. However, the distinction between intermediary and stratiform profiles is not necessarily unambiguous, as in Fig. 6(d). Our classification is only approximate. However, it captures the consistent, repeatedly observed features apparent in our inspection of the entire collection of profiles. Of the 93 profiles, 26 were classified as convective, 30 intermediary, and 37 stratiform. These numbers are not necessarily proportional to the area coverage of each type of precipitation, since the aircraft sampling strategy consisted of separate modules to sample convective and stratiform precipitation (Webster and Houze 1991).

Profiles of mean divergence, from the entire EMEX data set, for convective, intermediary, and stratiform areas are shown in Fig. 7. We have elected to display these mean profiles against pressure as the vertical coordinate in order to make clear the mass-balance constraint: the area under each divergence profile (including the unmeasured upper-tropospheric divergence) must be zero if vertical mass flux is zero at the top and bottom of the troposphere. Note that in all three types of precipitation, net convergence dominated within the measured levels, implying that there must be unmeasured divergence above 12 km, as is found in rawinsonde profiles (e.g. Fig. 11). In Fig. 8 the means have been subdivided according to the different types of MCSs observed in different synoptic environments within the monsoon (see Fig. 15 of Part I). The mean profiles share a basic similarity in all three types of MCSs.

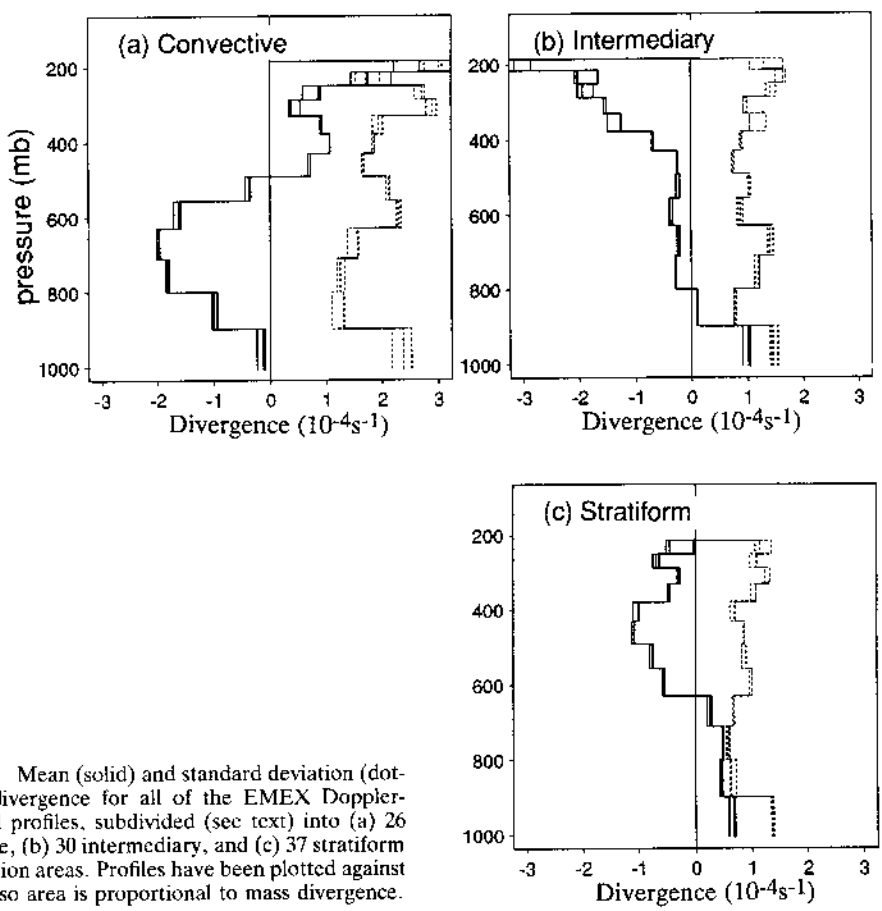

Figure 7. Mean (solid) and standard deviation (dotted) of divergence for all of the EMEX Doppler-measured profiles, subdivided (see text) into (a) 26 convective, (b) 30 intermediary, and (c) 37 stratiform precipitation areas. Profiles have been plotted against pressure so area is proportional to mass divergence.

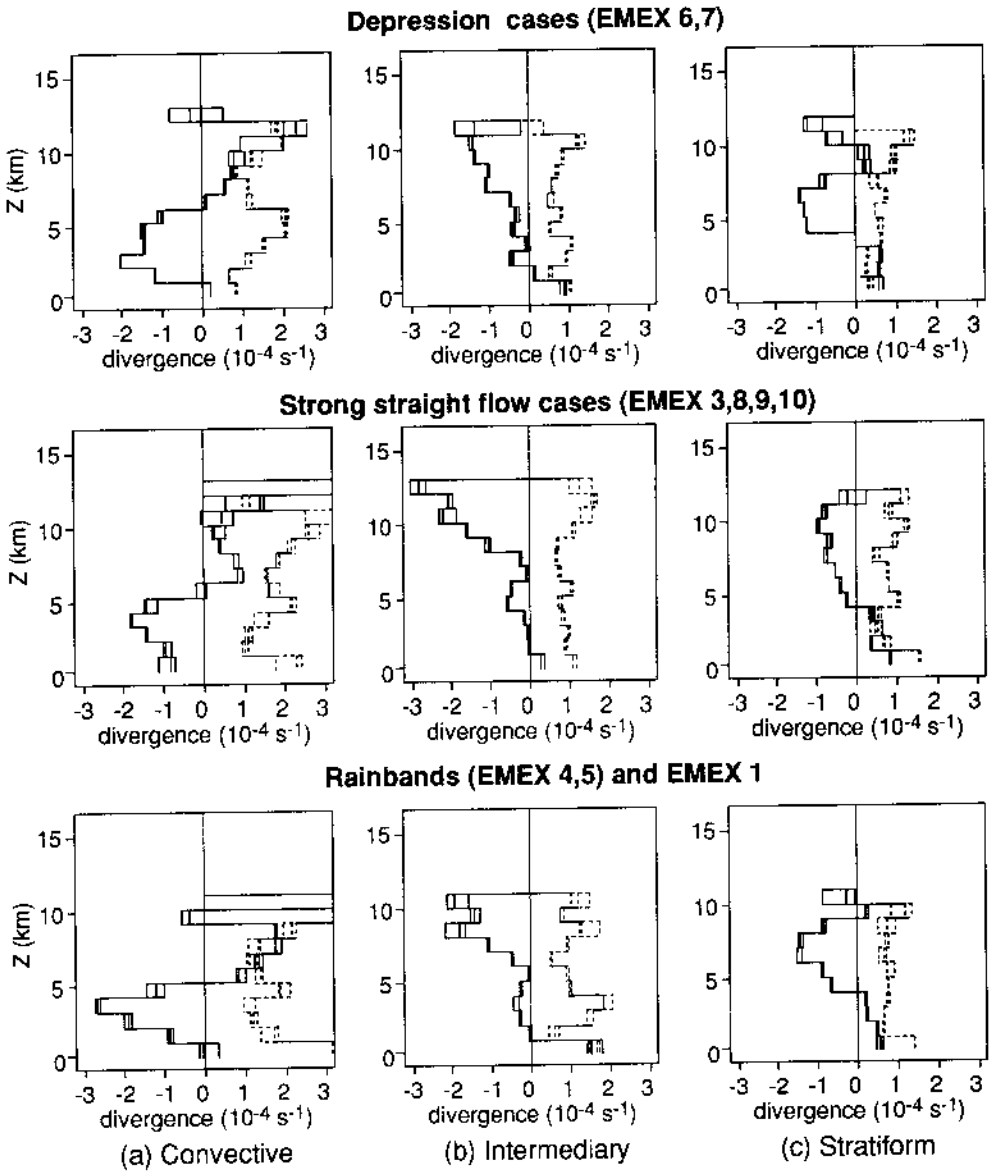

Figure 8. As in Fig. 7, except further subdivided according to the synoptic environment within which the MCSs were observed, and plotted against height.

In general, the standard deviations (dashed lines) are comparable with the value of the mean. However, the reader should by no means infer that the sign of mean divergence is everywhere uncertain. Differences among the three solid lines roughly delineate the envelope of sampling error associated with the Doppler-radar measurements themselves. Other sources of error include evolution of the flow during the sampling interval (hard to estimate), and errors in horizontal wind estimates due to incorrectly estimated particle fall speed (the contribution of assumed fall speed to divergence (see Eq. (3)) is shown on Figs. 6(a)–(e)). The remainder of the variance is meteorological, and is therefore not a measure of the validity of the means, but rather an additional quantity of interest.

(*i*) *Convective areas*. The convective-area mean profiles show convergence from the surface up to about 500 mb or 6 km, then divergence above that (Figs. 7(a) and 8(a)). The level of maximum convergence is elevated off the surface. It must be remembered that the sample represented here is of convective areas, identified by radar-reflectivity cells, in the mature stages of the MCS life cycle. Simple thermodynamic arguments suggest that much of the elevated convergence must feed into downdraughts, since this much mass of low equivalent potential temperature (θ_e) air entrained into updraughts would negate their buoyancy. Aircraft measurements of downdraught mass flux in deep convection (Fig. 3 of Jorgensen and LeMone 1989), while noisy, support the notion that convergence at 2–4 km altitude feeds into downdraughts. The weak *net* divergence at the surface is the integrated effect of the low-θ_e downdraught outflows and the high-θ_e air converging into updraughts. Some young convection was sampled, but overall the early growth stages of convective cells, when surface convergence might be higher, were probably undersampled.

A distinct maximum in the standard deviation of the convective divergence profiles, just below the crossover point at around 500 mb or 5 km (in Figs. 7(a) and 8(a) respectively), indicates that divergence at this level fluctuated more than at other levels. This may be related to the variations in the presence and strength of the isothermal layer often found near the 0°C level. The theory of Bretherton and Smolarkiewicz (1989) predicts that convection penetrating an environmental cold layer should entrain mass below and above the cold layer.

(*ii*) *Stratiform areas*. In the mean stratiform profiles divergence is observed below the 650 mb level, with convergence peaking at mid levels (6–7 km or ≈450 mb) above the melting level (Figs. 7(c) and 8(c)). The predominance of mass convergence in the measured profiles suggests that unmeasured divergence lay above this convergent layer. This divergence–convergence–divergence profile is common to the results of essentially all previous studies of MCS stratiform areas in the tropics and mid latitudes (Houze 1989). The fact that the convergent layer extends as high as it does may reflect contamination of the stratiform sample by intermediary profiles, with their upper-tropospheric convergence. Most of the stratiform profiles simply did not extend above 9 km, owing to radar attenuation, so the sample at 11 km is biased toward the deeper structures, which were younger and hence closer to the intermediary stage.

However, convergence extending up to 11 km was consistently found in the stratiform precipitation areas, both ahead of and behind the line of convection, in the MCS sampled on EMEX flight number 3. In that case, the strongest environmental winds were at mid levels, and the reflectivity field in the stratiform areas was eroded away at mid levels. To the extent that the mid-level convergence in the stratiform region is associated with cooling by sublimation or evaporation of hydrometeors at the base of the stratiform cloud deck, an elevated base of the cloud deck could explain the consistently elevated convergence in the EMEX flight 3 stratiform areas.

(*iii*) *Intermediary areas*. The mean intermediary precipitation-area divergence profiles (Figs. 7(b) and 8(b)), as foreshadowed by Fig. 6(c) above, are characterized by a convergence peak high in the troposphere, near the top of the data. The preponderance of mass convergence in the profile suggests that this convergence feeds into mean ascent in the upper troposphere, and that, as in the convective and stratiform areas, substantial unsampled divergence existed above about 250 mb. This upper-level convergence is a novel observation, and calls for some speculation about its physical significance.

The atmosphere cannot instantly accommodate a large amount of mass ascending in convective cells, whose level of neutral buoyancy is in a thin layer near the top of the troposphere. Initially, convective cells are thus forced (by a perturbation pressure-

gradient force opposing the buoyancy force) to detrain their mass flux over a deep layer of the upper troposphere (as observed in Figs. 7(a) and 8(a)), much of it below its level of neutral buoyancy. The resulting deep slab or lens of cloudy outflow air then gradually collapses in the vertical, and spreads out in the horizontal at its level of neutral buoyancy, as described by Lilly (1988). In the weakly stratified upper troposphere, below the highly stratified stratosphere, this collapse process would be asymmetrical, involving mostly upper-tropospheric ascent. This could explain the observed upper-level convergence observed in intermediary precipitation areas. Downward motions at tropopause level, just above the stratiform portions of MCSs, consistent with this hypothesized slumping and vertical collapse, are observed in both the tropics (Balsley *et al.* 1988) and mid latitudes (Johnson *et al.* 1990).

This process may be seen in a laboratory fluid in Fig. 1 of Mapes (1993), which shows a convective plume initially detraining in a single fat bulge, and then gradually separating into the thin detrainment layers which characterize the state of the fluid in the long-time limit, after several tens of buoyancy periods (corresponding to several hours in the tropical troposphere). Only in that limit can one assume that fluid parcels have at last found their levels of neutral buoyancy.

In this view, the upper-tropospheric ascent in the intermediary and stratiform precipitation areas is a continuation of the overall deep convective process in which high-θ_e air from low levels ascends to the level in the upper troposphere where it is neutrally buoyant. The air converging into the mid-tropospheric base of the mesoscale ascent in stratiform precipitation is apparently high-θ_e air which has previously diverged out of convective cells, since environmental mid-level air is absolutely stable. This mesoscale ascent simply occurs at a larger aspect ratio than the convective cells, and hence under slower, quasi-hydrostatic dynamics.

The 'hot tower' conceptual model of convection (Riehl and Malkus 1958) was devised as an explanation for the overall vertical transport in the tropics of low-level (high-θ_e) air through the mean mid-tropospheric θ_e minimum. In a sense, then, the term hot tower applies not just to convective cells, which happen to fit visually the description of a tower, but to MCSs in their entirety. MCSs do ultimately deliver a lot of high-θ_e air to the upper troposphere. However, it arrives only after spending several hours in the mid troposphere, at first rapidly ascending in towers, then slowly diverging outward and collapsing into an upper-tropospheric layer in the intermediary and stratiform stages of the convective process.

5. Inferences from rawinsonde divergence and vorticity profiles

(*a*) *Gulf of Carpentaria divergence profiles*

It seems likely that MCS-mean divergence profiles might have a stable, repeatable, physically determined mean, as the numerous updraughts and downdraughts contributing to Fig. 4 average out to give the stable mean convective, intermediary, and stratiform divergence profiles of Figs. 7 and 8. However, whole-MCS divergence profiles cannot be deduced from the Doppler-radar measurements alone, because the radar coverage in time and space was not adequate to determine the correct area-weighting of convective, intermediary, and stratiform profiles.

It should be noted, however, that no matter what proportions of mean convective, intermediary, and stratiform divergence profiles are added together, the resulting low-level convergence maximum is elevated off the surface. One major implication of this fact is that MCSs cause low-level upward displacements in the atmosphere surrounding them, thus creating more favourable conditions for the development of new convection

(Mapes 1993). The elevated convergence peak also has implications for the spin-up of tropical cyclones. A similar elevated convergence peak is also observed in mid-latitude MCSs (Fig. 7 of Maddox 1983).

The Doppler divergence profiles in various parts of MCSs would be complemented nicely by larger-scale measurements which illustrate whole-system, whole-lifetime divergence profiles for similar tropical MCSs. Unfortunately, the convection within the Gulf of Carpentaria sounding array (Fig. 1) was substantially less vigorous and organized than the EMEX aircraft-sampled MCSs, which were primarily over the Joseph Bonaparte Gulf and the Arafura Sea. Nevertheless, we have computed divergence profiles for the Gulf array by evaluating the line integral (1) with rawinsonde winds, interpolating the vector wind linearly between sounding sites. A mass-balance correction, constant with height, has been applied, since in our judgment the errors in wind interpolation exceed the error of the boundary conditions ($\omega = 0$ at surface and ~ 20 km). The resulting profiles are noisy, so some averaging is necessary.

Mean profiles of mass divergence over the Gulf of Carpentaria are shown in Fig. 9. Figure 9(a) shows mass divergence for five composite stages—formative, growing, mature, late, and decaying—of the MCS life cycle, in the four-MCS composite framework used by Frank and McBride (1989). Note that the low-level convergence in mature MCSs is elevated off the surface, just as indicated by the Doppler-radar measurements. Figure 9(b) shows mass divergence, for the four sounding times of day, averaged over the pre-cyclone active periods 15–17 Jan. and 30 Jan.–4 Feb. Again the low-level convergence peak is elevated, and an interesting kink in the profiles at 10 km is evident. This divergence minimum near 10 km is near the level of the convergence peak in the mean intermediary precipitation-area profiles and the slight secondary peak in the mean stratiform profiles in Figs. 7 and 8. It is also at this level that the static stability drops rapidly from its lower-tropospheric value to its smaller upper-tropospheric value. The meaning of these observations remains unclear.

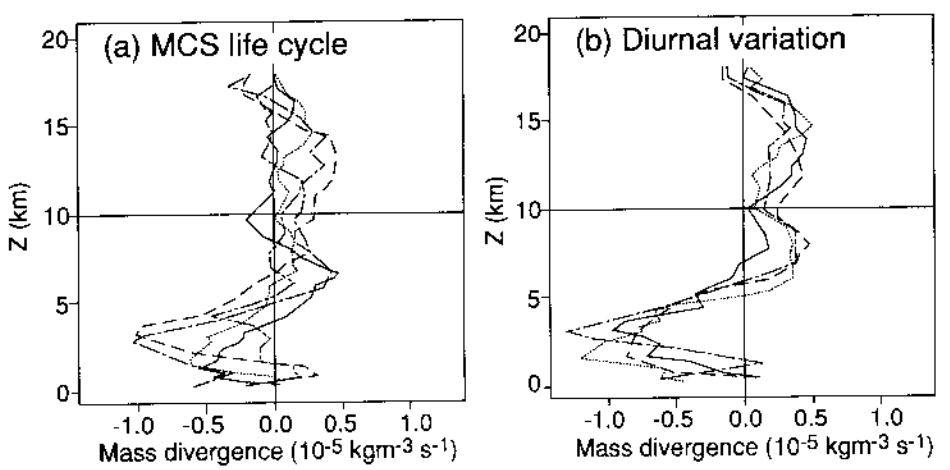

Figure 9. Rawinsonde-derived corrected mean mass divergences in the Gulf of Carpentaria. (a) The five stages of the MCS life cycle, for the composite of four MCSs, after Frank and McBride (1989). 'Initial' stage (solid), 'growth' stage (dotted), 'maximum intensity' stage (dash-dotted), 'early decay' (dashed), 'late decay' stage (dash-double-dotted). (b) The four sounding times per day averaged over the non-cyclone active days, 15–17 Jan. and 30 Jan.–4 Feb. 1987. 05 GMT (afternoon) solid, 11 GMT (nightfall) dotted, 17 GMT (after midnight) dashed, 23 GMT (dawn) dash-dotted.

(*b*) *Gulf of Carpentaria vorticity profiles*

Further evidence of an elevated convergence maximum in monsoon MCSs can be found in vorticity profiles. Neglecting the intermittent vortex couplets caused by MCS momentum transports (see section 3 and Part I for discussion), the vertical profile of vorticity can be loosely interpreted as a time-integrated measure of the divergence profiles of monsoon MCSs.

Profiles of vorticity calculated from the Gulf of Carpentaria rawinsonde array are shown in Fig. 10. Low-level cyclonic circulation in the pre-cyclone periods (Fig. 10(a)) had its maximum at 3–5 km altitude, consistent with the measurements (Figs. 6–9) of similarly elevated convergence in MCSs. Davidson *et al.* (1990) also found that elevated cyclonic vorticity maxima preceded the formation of cyclones Irma and Jason in the 1987 Australian monsoon. As the cyclones intensified, the level of maximum circulation descended to near the surface (Fig. 10(b)), in agreement with the findings of Davidson *et al.* (1990). This surface spin-up evidently reflects the transition from a regime of vortex stretching by the elevated convergence typical of MCSs, to a regime of vortex stretching by the strong surface inflow associated with the secondary circulation of the intensifying cyclone.

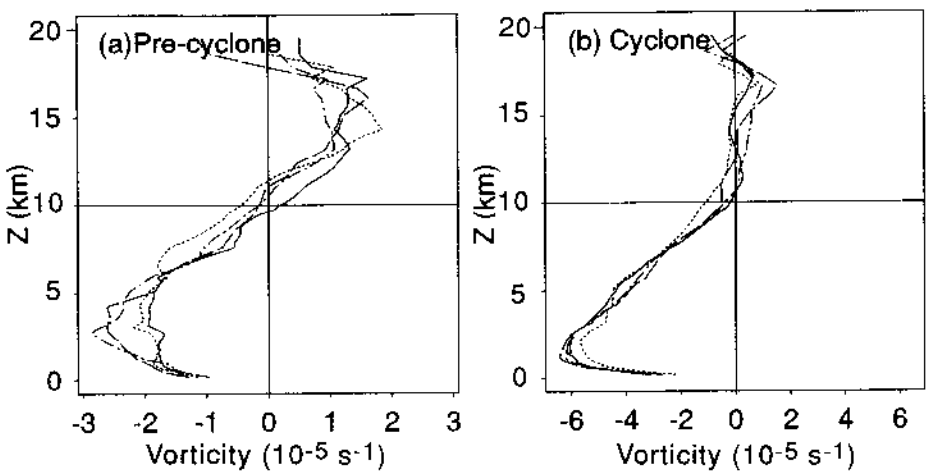

Figure 10. Vorticity profiles for the Gulf of Carpentaria. The four curves are for the four times of day (05, 11, 17, 23 GMT, as in Fig. 9(b)). (a) Pre-cyclone active periods 15–17 Jan. and 30 Jan.–4 Feb. 1987. (b) Cyclone periods 18–20 Jan. and 7–13 Feb. 1987.

(*c*) *Monsoon vertical structure as a function of scale*

Vorticity and divergence profiles on a larger scale have been calculated from the whole north Australian sounding array (heavy dots on Fig. 1), which surrounded the mean monsoon trough at low levels (Fig. 3 of Part I). The time-mean profiles from all of AMEX Phase II are shown in Fig. 11, and compared with the time-mean Gulf of Carpentaria profiles. Over the Gulf the convergent and cyclonic lower layer of the monsoon extended to about 11 km height. On the larger scale of all north Australia, however, the vertical structure of both divergence and vorticity was more nearly symmetric through the troposphere and more nearly approximating the 'gravest vertical mode' of the troposphere.

Geostrophic adjustment theory as applied to a heated rotating stratified fluid (e.g. Gill 1982) predicts that the effects of a heat source are confined within an e-folding

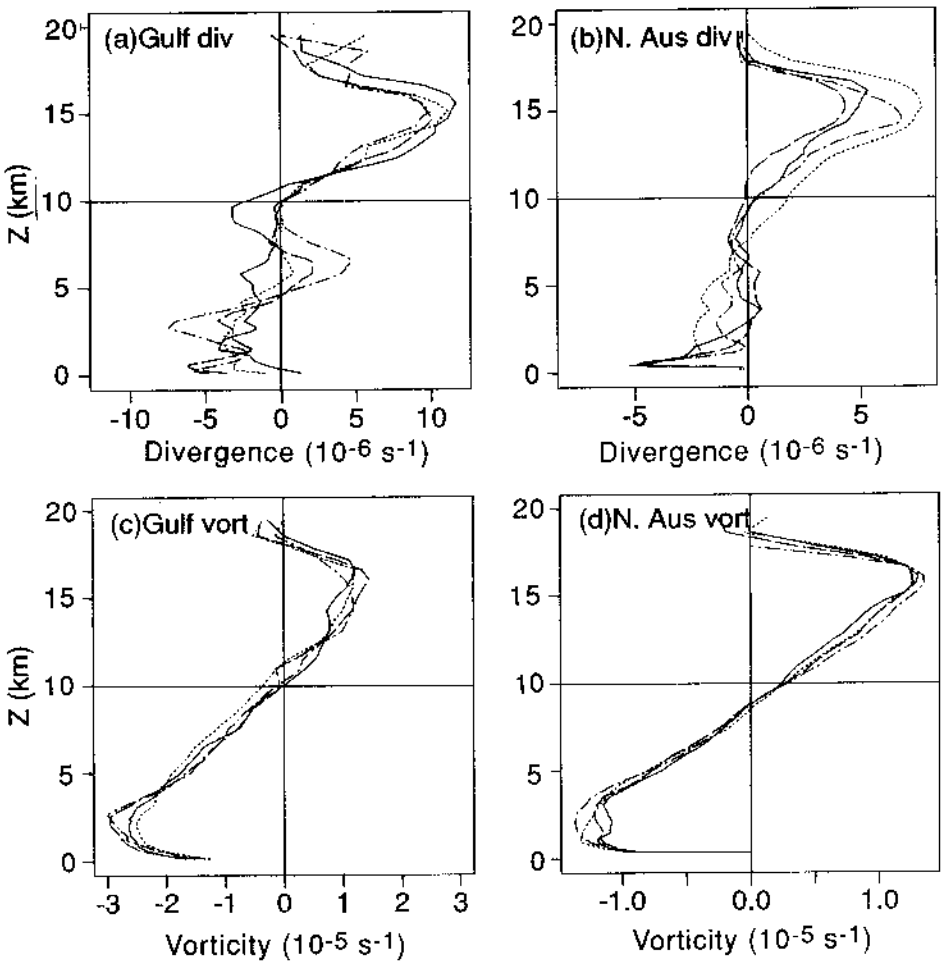

Figure 11. Mean divergence and vorticity profiles, during all of AMEX (14 Jan.–15 Feb. 1987) for the Gulf of Carpentaria (left) and larger north Australia (right) rawinsonde arrays. The four curves are the four times of day as in Fig. 9(b).

distance known as the Rossby radius of deformation. For a heat source with a vertical profile which excites several vertical modes, there are several Rossby radii, the smaller vertical modes having smaller Rossby radii. The shallower vertical structures excited by a complex heating profile are only observed out to a small distance away from the heating, while the deeper vertical structures affect larger horizontal areas (for a mechanistic discussion, see Mapes (1993)).

The gravest mode of the troposphere (convergence in the lower troposphere, divergence aloft, half a wavelength spanning the troposphere) is strongly excited by the convective portions of MCSs. The second mode, with one wavelength spanning the troposphere, is strongly excited by stratiform precipitation, with its three-layered divergence profile, corresponding to cooling in the lower troposphere and heating aloft (Houze 1989). Numerical values of Rossby radii (cf. Gill 1982) at 15° latitude are approximately 1000 km for the 30 km gravest mode of the troposphere and 500 km, comparable with the size of the north Australian rawinsonde array, for a 15 km vertical wavelength. Hence 15 km and shallower flow structures should be mostly (e^{-1}) trapped within the array, and

not observed in wind measurements at the perimeter. The observations in Fig. 11 are in qualitative agreement with those predictions.

This trapping of shallow vertical structures at small horizontal scales underlies the success of simple shallow-water or two-level models in simulating the large-scale horizontal structure of wind fields forced by tropical heat sources (e.g. Gill 1980; Silva Dias *et al.* 1983). All heating profiles positive through the troposphere project strongly onto the gravest baroclinic mode (DeMaria 1985; Fig. 6 of Salby and Garcia 1987), and it is this gravest mode which dominates the horizontal wind-field maps. However, the superposition of vertical modes of different scales is extremely important for modelling the vertical structure of wind fields (Hartmann *et al.* 1984), and low-level convergence fields which so strongly affect the development of new convection (Chang and Lim 1988; Mapes 1992). Tropical cyclogenesis is also apparently a problem which involves complex vertical structure at low levels (Fig. 10). Reliable, direct measurements of the mean divergence profiles of MCSs in their entirety are needed to address these important questions.

6. Summary and conclusions

The 1987 Australian monsoon was a circulation primarily forced by heating in its embedded convection.* In the tropical troposphere, temperature varies little in the horizontal and in time, so this convective heating may be profitably viewed as a mass source (divergence) in the upper troposphere, where θ is high, and a mass sink (convergence) in the lower troposphere, where θ is low. In the vorticity equation 'thermal forcing' appears as horizontal divergence. Furthermore, divergence is a measurable quantity, which underlies diagnoses of heating. For these reasons we have focused in this study on divergence profiles rather than heating profiles. We thus avoid the vertical smearing of errors, and the de-emphasis of well-measured, but shallow, divergence features which occur when divergence measurements are integrated vertically to yield estimates of vertical velocity or heating.

Precipitation features within an MCS undergo an evolution from cellular convective structure, through intermediary structure, to stratiform precipitation structure. Ninety-three divergence profiles, within convective, intermediary, and stratiform portions of nine diverse MCSs, have been measured with airborne Doppler radar. The divergence profiles of the convective, intermediary, and stratiform precipitation areas, which together constitute MCSs, are surprisingly similar from case to case and from one synoptic environment to another (Fig. 8).

Convective profiles are characterized by convergence from the surface to 5–6 km, with its maximum value at 2–4 km, and divergence above 6 km. The elevated peak in convergence is apparently indicative of strong convective downdraught activity. Intermediary profiles are characterized by upper-tropospheric convergence with its maximum at the highest levels to which the radar data reach (11–12 km). Mass-balance constraints imply that this converging air feeds into upward motion high in the upper troposphere. Stratiform profiles show divergence below 4 km, and convergence from 4–8 km or more. Again mass balance indicates divergence above the top of the sampled levels. Apparently convective cells detrain their upward mass flux in a deep slab in the upper troposphere. This deep layer then slowly (quasi-hydrostatically) collapses upward, in the intermediary

* This statement is a premise, not a result, of the present study. K. Puri (personal communication) has obtained realistic simulations of the 1987 Australian monsoon wind fields by specifying a heat source wherever satellite imagery shows that a cloud cluster actually existed.

and stratiform stages of evolution, as the surrounding atmosphere accommodates itself to the convective intrusion of air whose level of neutral buoyancy is in the upper troposphere. Mid-level convergence and low-level divergence in the stratiform profile indicate the development of a lower-tropospheric mesoscale downdraught associated with the melting evaporation of stratiform rain.

These Doppler divergence profiles indicate that, no matter what the proportions of convective, intermediary, and stratiform precipitation, *the net low-level convergence into monsoon MCSs peaks at a level elevated off the surface*. Rawinsonde-derived divergence profiles are in agreement (Fig. 9). This elevated convergence (also seen in mid-latitude convection (Maddox 1983)) has important consequences for both the divergent and rotational flows induced by MCS heating. The elevated convergence peak causes low-level upward displacements in the environment of MCSs, which favours additional convective development. The result is that monsoon convection is gregarious: the MCSs occur in 'superclusters' (Mapes 1993). Another apparent consequence of elevated convergence is the elevated cyclonic vorticity maximum in the monsoon trough and depressions before tropical cyclone formation (Fig. 10, Davidson *et al.* 1990).

Divergence and vorticity profiles in the monsoon show an upscale simplification: the flow on larger horizontal scales is increasingly dominated by deeper, simpler vertical structure, consistent with the predictions of geostrophic adjustment theory.

Acknowledgements

Thanks to Nancy Figueroa of the Hurricane Research Division (HRD) for help in preprocessing of the Doppler-radar data. Chungli Wang performed much of the Doppler data analysis. G. C. Gudmundson edited the original manuscript. The EMEX P3 aircraft operations were directed by Drs R. Burpee and F. Marks of the HRD. This work was supported by the US NOAA (HRD) and National Science Foundation, under NSF grant ATM9008406 and by the US National Aeronautics and Space Administration grants NAG51599 and NAGW2633.

References

Balsley, B. B., Ecklund, W. L., Carter, D. A., Riddle, A. C. and Gage, K. S. 1988 Average vertical motions in the tropical atmosphere observed by a radar wind profiler on Pohnpei (7°N latitude, 157°E longitude). *J. Atmos. Sci.*, **45**, 396–405

Bretherton, C. S. and Smolarkiewicz, P. K. 1989 Gravity waves, compensating subsidence, and detrainment around cumulus clouds. *J. Atmos. Sci.*, **46**, 740–759

Chang, C.-P. and Lim, H. 1988 Kelvin wave-CISK: a possible mechanism for the 30–50 day oscillations. *J. Atmos. Sci.*, **45**, 1709–1720

Davidson, N. E., Holland, G. J., McBride, J. L. and Keenan, T. D. 1990 On the formation of AMEX cyclones Irma and Jason. *Mon. Weather Rev.*, **118**, 1981–2000

DeMaria, M. 1985 Linear response of a stratified tropical atmosphere to convective heating. *J. Atmos. Sci.*, **42**, 1944–1959

Frank, W. M. and McBride, J. L. 1989 The vertical distribution of heating in AMEX and GATE cloud clusters. *J. Atmos. Sci.*, **46**, 3464–3478

Gill, A. E. 1980 Some simple solutions for heat-induced tropical circulation. *Q. J. R. Meteorol. Soc.*, **106**, 447–462

1982 *Atmosphere–ocean dynamics*. Academic Press, San Diego

Gunn, B. W., McBride, J. L., Holland, G. J., Keenan, T. D. and Davidson, N. E. 1989 The Australian summer monsoon circulation during AMEX Phase II. *Mon. Weather Rev.*, **117**, 2554–2574

Hartmann, D. L., Hendon, H. H. and Houze, Jr., R. A. 1984 Some implications of mesoscale circulations in tropical cloud clusters for large-scale dynamics and climate. *J. Atmos. Sci.*, **41**, 113–121

Houze, Jr., R. A.	1982	Cloud clusters and large-scale vertical motions in the tropics. *J. Meteorol. Soc. Japan*, **60**, 396–410
	1989	Observed structure of mesoscale convective systems and implications for large-scale heating. *Q. J. R. Meteorol. Soc.*, **115**, 425–461
Johnson, R. H., Gallus, W. A. and Vescio, M. C.	1990	Near-tropopause vertical motion within the trailing stratiform region of a midlatitude squall line. *Mon. Weather Rev.*, **110**, 1898–1911
Jorgensen, D. P. and LeMone, M. A.	1989	Vertical velocity characteristics of oceanic convection. *J. Atmos. Sci.*, **46**, 621–640
LeMone, M. A.	1983	Momentum transport by a line of cumulonimbus. *J. Atmos. Sci.*, **40**, 1815–1834
Lilly, D. K.	1988	Cirrus outflow dynamics. *J. Atmos. Sci.*, **45**, 1594–1605
Maddox, R. A.	1983	Large-scale meteorological conditions associated with midlatitude MCCs. *Mon. Weather Rev.*, **103**, 1475–1493
Mapes, B. E.	1993	Gregarious tropical convection. *J. Atmos. Sci.*, in press
Mapes, B. E. and Houze, Jr., R. A.	1992	An integrated view of the 1987 Australian monsoon and its mesoscale convective systems. I: Horizontal structure. *Q. J. R. Meteorol. Soc.*, **118**, 927–963
Marks, F. D. and Houze, Jr., R. A.	1987	Inner core structure of hurricane Alicia from airborne Doppler-radar observations. *J. Atmos. Sci.*, **44**, 1296–1317
Riehl, H. and Malkus, J. S.	1958	On the heat balance in the equatorial trough zone. *Geophysica*, **6**, 503–538
Salby, M. L. and Garcia, R. R.	1987	Transient response to localized episodic heating in the tropics. Part I: Excitation and short-time near-field behavior. *J. Atmos. Sci.*, **44**, 458–498
Sardeshmukh, P. D. and Held, I. M.	1984	The vorticity balance in the tropical upper troposphere of a general circulation model. *J. Atmos. Sci.*, **41**, 768–777
Sardeshmukh, P. D. and Hoskins, B. J.	1985	Vorticity balances in the tropics during the 1982–83 El Niño–Southern Oscillation event. *Q. J. R. Meteorol. Soc.*, **111**, 261–278
	1987	On the derivation of the divergent flow from the rotational flow: the chi-problem. *Q. J. R. Meteorol. Soc.*, **113**, 339–360
	1988	The generation of global rotational flow by steady idealized tropical divergence. *J. Atmos. Sci.*, **45**, 1228–1251
Silva Dias, P. L., Schubert, W. H. and DeMaria, M.	1983	Large-scale response of the tropical atmosphere to transient convection. *J. Atmos. Sci.*, **40**, 2689–2707
Srivastava, R. C., Matejka, T. J. and Lorello, T. J.	1985	Doppler-radar study of the trailing anvil region associated with a squall line. *J. Atmos. Sci.*, **43**, 356–377
Webster, P. J. and Houze, Jr., R. A.	1991	The Equatorial Mesoscale Experiment (EMEX): An overview. *Bull. Am. Meteorol. Soc.*, **72**, 1481–1505